



Determination of the Drag Reduction Mechanism Associated with the Pneumatic Regulation of Slurry Pipeline Transport using a Numerical Method

Q. Y. Chen¹, T. Xing¹, Q. Wu¹, W. Wei¹, W. Zhang², P. Jiang^{1†}

¹ Wuhan University of Technology, Wuhan, Hubei, 430063, China

² WenHua College, Wuhan, Hubei, 430074, China

†Corresponding Author Email: cqy_dawn@163.com

(Received October 25, 2018; accepted January 22, 2019)

ABSTRACT

The technological parameters associated with the pneumatic regulation of slurry pipeline transport have been explored to reduce the energy consumption of the transport system and prolong the transport distance in dredging cases. In this study, a numerical method is employed to discretize and solve the established three-dimensional physical model, which consists of a dual Eulerian model of multiphase flow, the standard $k-\varepsilon$ model of turbulence, and a homogeneous flow model for slurry. The simulated pressure drop values are consistent with the experimental results for transport with gas injection. In addition, the influence of the gas phase on the flow characteristics in the pipeline is analyzed, and the mechanism of the drag reduction is revealed. The presence of the gas film reduces the wall shear stress between the slurry and the pipe wall, which is the root cause of the drag reduction. Under the control of pneumatic regulation, the flow state tends to stabilize in the fully developed section of the pipe, and injection does not interfere with transport.

Keywords: Piping; Numerical simulation; Slurry; Two-phase flow; Turbulent flow.

NOMENCLATURE

A_c area of the pipe section	u velocity in the x direction
A_w wall contact area	V volume
C_v slurry concentration	V_a gas velocity
C_f friction coefficient	V_s slurry velocity
D diameter of the main pipe	v velocity in the y direction
D_f friction drag force	w velocity in the z direction
d diameter of the branch pipe	x x component in the coordinate system
G_b turbulent kinetic energy due to buoyancy	y y component in the coordinate system
G_k turbulent kinetic energy due to the average velocity gradient	z z component in the coordinate system
g gravitational constant	α air ejection angle
K diffusion coefficient	β thermal expansion coefficient
k turbulent kinetic energy	ε turbulent dissipation
L_1 length of the main pipe	μ_t turbulent viscosity
L_2 length of the head pipe section	ρ density of liquid
Pr turbulent Prandtl number	ρ_l local average density
S_ϕ source term includes the sources of enthalpy	σ_ε Prandtl numbers corresponding to the turbulent dissipation rate
S_ε source terms of ε	
S_k source terms of k	
T temperature	
U fluid transient velocity	
U_w flow velocity at the wall	

Subscripts

t time

i space index in the horizontal direction
 Δt time step

j space index in the vertical direction

1. INTRODUCTION

Slurry pipeline transport is widely used in dredging, chemical industries and other fields. Slurry has a high specific gravity, low flow velocity and high viscosity, which can cause serious problems during transport, such as generating frictional resistance at the wall and decreasing the effective transport distance (Miedema, 2016). However, pneumatic regulation technology, as auxiliary technology, can be applied for slurry pipeline transport to effectively reduce the associated drag, extend the transport distance and save energy.

Gas-assisted transport was first performed in the chemical industry. When a high concentration of a non-Newtonian fluid, such as water with clay, was transported with injected gas, the pressure inside the pipe dropped (Lockhart & Martinelli, 1949). The injection of gas reduced the internal friction in the pipe when conveying the shear-thinning fluid. As a result, the pressure gradient was reduced, and drag reduction was achieved (Srivastava & Narasimhamurty, 1973). These studies indicate that gas-assisted transport can reduce drag under certain conditions, but specific methods have not been proposed. Based on a series of experiments, a theoretical system was clearly developed for gas-assisted transport. Four fluid states of gas-liquid two-phase flow were summarized, and a mathematical model was established by analyzing the pressure gradient drop for gas-liquid two-phase flow in a smooth horizontal pipeline (Hoogendoorn, 1959). Then, to analyze the effects of gas on the flow resistance of the pipeline, the pressure gradient was compared between the gas-liquid two-phase flow and the single-phase liquid. A metric for evaluating the drag reduction effect was proposed based on the pressure gradient (Heywood & Charles, 1979). According to the metric, Gillies built a pipeline test apparatus to investigate the liquid carrying capacity and proposed that gas can improve the transport capacity of sand carried by water under turbulent conditions (Gillies, Mckibben, & Shook, 1996). Orell improved the two-phase flow model by considering the sedimentation of solid particles and the sliding of the fluidized bed. A gas-liquid-sand three-phase flow model was proposed, and the model expanded the range of the two-phase flow model (Orell, 2005, 2007). In addition, as gas-assisted transport models have improved, gas-assisted transport has become increasingly applied to other types of pipeline

transport. In the livestock industry, Bjerkholt established a set of gas-assisted pipeline transport apparatuses to help convey pig and cattle feces (Bjerkholt, Cumby, & Scotford, 2005). All these studies confirmed that injecting gas is conducive to transport under certain conditions. However, the corresponding experimental analyses have some limitations because many of the flow parameters are difficult to accurately and rapidly obtain.

Computational fluid dynamics (CFD)-based methods have become increasingly popular for investigating various multiphase fluid flow problems in closed conduits and open channels. One advantage of a CFD-based approach is that three-dimensional solid-liquid two-phase flow problems can be rapidly simulated under wide ranges of flow conditions and sediment characteristics, which is almost impossible experimentally. Among the CFD calculation models, the Eulerian multiphase flow model is the most widely used in pipeline transport. The Eulerian multiphase flow model can not only simulate high concentrations of homogenous slurry in straight pipes (Kaushal, Thinglas, Tomita, Kuchii, & Tsukamoto, 2012) but also describe suspended particle behaviors at low concentrations (Messa & Malavasi, 2015; Messa, Malin, & Malavasi, 2014). Moreover, different flow characteristics can be accurately described during slurry transport (Gopaliya & Kaushal, 2015). In addition, gas-liquid two-phase flow at low gas flow rates can be simulated based on the Eulerian model (Ali & Pushpavanam, 2011).

To rapidly obtain the flow characteristics, a high-order, fully conservative CFD code based on the Eulerian model is proposed for gas-assisted transport. Furthermore, the influences of the air ejection angle and gas velocity on drag reduction are investigated, and the parameter intervals and theory of drag reduction are discussed.

2. NUMERICAL METHOD

In this study, the slurry conveyed in the pipeline forms a homogeneous flow, so a homogeneous flow model is adopted. Ignoring the effects of individual particles, the liquid–solid slurry is mathematically treated as a continuum. In addition, the density and apparent viscosity of the continuum are equal to those of the actual slurry in calculations. Therefore, slurry transport with air ejection can be simplified as a two-phase flow.

The Eulerian two-phase flow model is used in this study, and the continuity equation and momentum equation are set simultaneously. The finite volume method and the standard $k-\varepsilon$ two equation model are also used. The SIMPLE algorithm based on solving for the pressure is used to couple the pressure term and the interface exchange coefficient to evaluate each phase.

2.1 Finite Volume Method and Governing Equations

The slurry transported by the pipeline is a multiphase fluid, so the convection-diffusion equation is solved by the finite volume method, which can effectively solve Euler equations in three-dimensional models (Jameson & Mavriplis, 1985). The finite volume method establishes a discrete equation based on the integral equation of the conservation of the fluid flow. This method establishes a discrete incompatible control volume around grid points and integrates the corresponding partial differential equations to determine each control volume; thus, a series of discrete equations is obtained. The conservative partial differential equations of the three-dimensional convection-diffusion equation are as follows:

$$\frac{\partial(\rho\varphi)}{\partial t} + \frac{\partial(\rho u\varphi)}{\partial x} + \frac{\partial(\rho v\varphi)}{\partial y} + \frac{\partial(\rho w\varphi)}{\partial z} = \frac{\partial}{\partial x}\left(K\frac{\partial\varphi}{\partial x}\right) + \frac{\partial}{\partial y}\left(K\frac{\partial\varphi}{\partial y}\right) + \frac{\partial}{\partial z}\left(K\frac{\partial\varphi}{\partial z}\right) + S_\varphi \quad (1)$$

where ρ is the reference fluid density; φ is related to convective diffusion, such as for heat or a concentration; t is the total time; u , v and w are the velocity components in the x , y and z directions, respectively; K is the diffusion coefficient; and S_φ is a source term that includes the sources of enthalpy. The formula above can be represented by divergent operators and gradients, as shown in Eq. (2).

The following formula can be obtained by integrating the control volume (CV) from the equation above in time step Δt :

$$\int_{CV} \left(\int_t^{t+\Delta t} \frac{\partial}{\partial t}(\rho\varphi) dt \right) dV + \int_t^{t+\Delta t} \left(\int_A n \cdot (\rho u\varphi) dA \right) dt = \int_t^{t+\Delta t} \left(\int_A n \cdot (K \text{grad} \varphi) dA \right) dt + \int_t^{t+\Delta t} \int_{CV} S_\varphi dV dt \quad (3)$$

where the divergence integral is changed to an area integral by Green's theorem (Casas & Fernández, 1989) and A is the surface area of the control volumes. Eq. (3) indicates that $\rho\varphi$ in the control volume CV and the flow rate $\rho\varphi$ through the surface of the CV during Δt can be combined to determine

the diffusion through the surface of the CV during Δt . Additionally, the changes in the source terms in the CV during Δt must also be considered.

2.2 Turbulence Equations

The air-assisted slurry transport case studied in this paper has a turbulent flow regime, so the standard $k-\varepsilon$ two-equation model is used for calculations and analysis.

The $k-\varepsilon$ transport equations for each phase are expressed as follows.

$$\frac{\partial(\rho k)}{\partial t} + \frac{\partial(\rho \mu_i k)}{\partial x_i} = \frac{\partial}{\partial x_j} \left[\left(\mu + \frac{\mu_i}{Pr_k} \right) \frac{\partial k}{\partial x_j} \right] + G_k + G_b - \rho \varepsilon + S_k \quad (4)$$

$$\frac{\partial(\rho \varepsilon)}{\partial t} + \frac{\partial(\rho \mu_i \varepsilon)}{\partial x_i} = \frac{\partial}{\partial x_j} \left[\left(\mu + \frac{\mu_i}{\sigma_\varepsilon} \right) \frac{\partial \varepsilon}{\partial x_j} \right] + \frac{\varepsilon}{k} (C_{\varepsilon 1} G_k - C_{\varepsilon 2} \rho \varepsilon + C_{\varepsilon 3} G_b) + S_\varepsilon \quad (5)$$

Then, the values of k and ε are substituted into Eq. (6) to calculate the turbulent viscosity, and the turbulent viscosity μ_t is obtained as follows.

$$\mu_t = \rho C_\mu k^2 / \varepsilon \quad (6)$$

G_k represents the turbulent kinetic energy induced by the average velocity gradient and can be expressed as follows.

$$G_k = \mu_t \frac{\partial u_i}{\partial x_i} \left(\frac{\partial u_j}{\partial x_i} + \frac{\partial u_i}{\partial x_j} \right) \quad (7)$$

G_b represents the turbulent kinetic energy induced by the effects of buoyancy.

$$G_b = \beta g_i \frac{\mu_t}{Pr_t} \frac{\partial T}{\partial x_i} \quad (8)$$

β is the thermal expansion coefficient for an incompressible fluid, i.e., when $G_b=0$; $-\rho\varepsilon$ is a dissipative term; $C_{\varepsilon 1} \varepsilon P_k / K$ is a term related to ε ; $C_{\varepsilon 1} \varepsilon C_{\varepsilon 3} G_b / K$ is the correction term of buoyancy; $-C_{\varepsilon 2} \rho \varepsilon^2 / K$ is the dissipative term; and S_k and S_ε are the source terms of k and ε , respectively. Default values of 0.09, 1.0, 1.44, 1.92 and 1.3 are selected for C_μ , Pr_k , $C_{\varepsilon 1}$, $C_{\varepsilon 2}$ and σ_ε , respectively. In addition, the range of i and j is (1, 2).

2.3 Drag Equation

The formula for the friction drag of the pneumatically conveyed slurry is as follows:

$$D_f = \frac{1}{2} C_f \rho_l (U_w - U)^2 A_w \quad (9)$$

where D_f and C_f are the frictional drag force and friction coefficient, respectively; ρ_l is the local average density; and U_w is the flow velocity at the wall. The friction coefficient, which is a nondimensional number used to determine the local resistance, can be defined as follows:

$$C_f = \tau / \rho_l \frac{U^2}{2} \quad (10)$$

where τ is the wall shear stress. There is a linear relationship between the friction coefficient and the wall shear stress. A decrease in the wall shear stress reduces the drag. In addition, drag reduction can be achieved by reducing the slip velocity ($U_w - U$) and the wall contact area A_w . Reducing the local average density ρ_l causes the friction coefficient C_f to increase. The average density has some relationship with flow velocity, so it is generally not regarded as a drag reduction factor.

If the slip speed is constant, the injection of bubbles around the wall reduces the local average density of the fluid, and the resistance can be reduced. This phenomenon, which is called the inertial effect of drag reduction, has a major influence on the turbulent flow regime (Marié, 1987). The presence of large bubbles close to the wall can reduce the area of wall contact. Replacing the liquid phase with the air phase in the boundary layer almost eliminates all drag, and only the friction of air, which is small compared to the friction of liquid, must be considered (Sanders, Winkel, Dowling, Perlin, & Ceccio, 2006). The two points noted above are discussed in detail in this paper.

In pipeline transport, the generation and ejection of high-pressure air reduces the contact area between the slurry and the pipe wall, and the continuity equation of the constant flow for an incompressible fluid is given as follows:

$$UA_c = Const \quad (11)$$

where U is the fluid velocity and A_c is the area of the pipe section. An increase in the slurry velocity leads to an increase in the pressure drop. Additionally, the presence of air can reduce the friction between the slurry and the wall, which causes a reduction in the wall shear stress (Aliseda & Lasheras, 2006). The relations noted above are the decisive factors that influence the resistance of pneumatic transport.

3. SIMULATION METHOD

3.1 Physical Model

The horizontal pipe section analyzed in this paper is

taken from a dredging pipe with an inner diameter of 219 mm. The physical model includes the main pipe for conveying the slurry and a branch pipe for injecting air. As shown in Fig. 1, the main pipe length is 20 meters, and the inner diameter of the main pipe is 219 mm. The junction of the branch pipe and the main pipe is located 2.35 meters from the left end of the main pipe. The diameter of the branch pipe is 90 mm, and the intersecting angle with the main pipe varies between 5° and 90°.

A O-grid block is built for fluid domains using ICEM CFD. To fully capture the spatial scale information associated with turbulence, a 20-layer exponentially growing boundary layer is established with a growth ratio of 1.2. Mesh-independent verification is performed, and the number of grids reaches 370K cells.

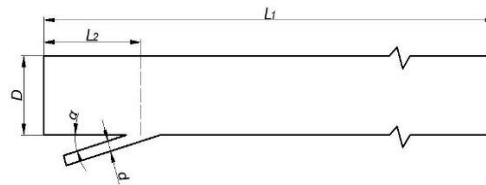


Fig. 1. Schematic view of the geometric model.

3.2 Boundary Conditions

A velocity inlet boundary condition is applied at each inlet. Specified values are assigned to the velocities of both phases: the slurry velocity in the main pipe is 1 m·s⁻¹, and the gas velocity in the branch pipe varies between 0.5 m·s⁻¹ and 2.5 m·s⁻¹. The air ejection angle of the branch pipe is between 5° and 40°. The default values of 5%, 10, and 20 °C are selected for the intensity of turbulence, turbulent viscosity ratio, and temperature, respectively. A pressure outlet boundary condition at atmospheric pressure is applied at the outlet.

A no-slip condition is applied at the wall, i.e., the velocity of the fluid phase close to the wall is set to zero, and the wall roughness is set as 0.02 mm. The models of Gidaspow and Lun are used for the granular viscosity and radial distribution of flow (Gidaspow, Bezburuah, & Ding, 1991; Lun, Savage, Jeffrey, & Chepurmy, 2006).

3.3 Solution Process and Convergence Scheme

A high-order, fully conservative CFD code tailored for turbulent flow computations is selected in this study to solve the governing equations with the boundary conditions discussed above. Root mean square residuals are used for the evaluation, and the

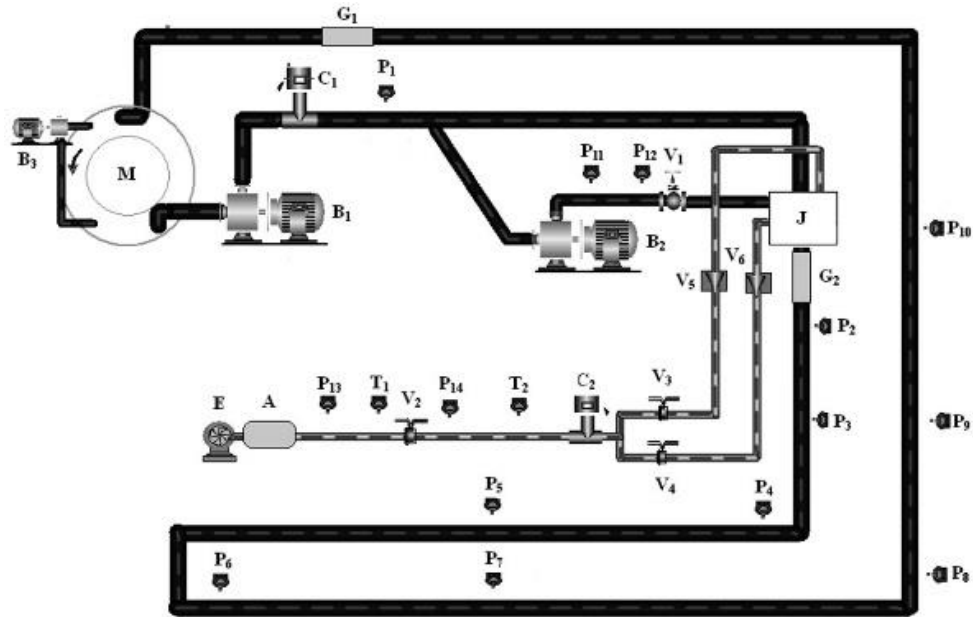


Fig. 2. Experimental pipeline apparatus.

residual for convergence is set as 10^{-4} . The phase-coupled SIMPLE algorithm is applied to ensure that the results are stable and accurate and that convergence is obtained. The QUICK method is adopted to solve the momentum equations. The pressure relaxation factor and momentum relaxation factor are set to 0.3 and 0.2, respectively, and the default values of the remaining factors are used. The time step is set as 0.01 s, and the total time distribution of the flow variables is calculated in 25 seconds.

4. RESULTS AND DISCUSSION

4.1 Validation of the Model

To improve the quality of the model and ensure the accuracy of the simulation, it is necessary to verify the simulation model with experimental data. The pipeline apparatus used to test the air-ejecting transport effect is shown in Fig. 2. This apparatus can work with different mass flow rates of gas, slurry concentrations and slurry velocities.

(A. Compressed air bottle; B1-B3. Different types of centrifugal pumps; C1-C2. Electromagnetic flowmeters; G1-G2. PMMA tubes; J. Nozzle; M. Slurry pool; P1-P14. Pressure gauges at different positions; T1-T2. Thermometers; V1. Flow control diaphragm valve; V2-V4. Gas valves; V5-V6. Non-return valve. The dark, thick tube is the main section of slurry flow, and the shallow, thin tube is the air ejection pipe section.)

The pipeline apparatus can be divided into the main

slurry pipeline system and the air ejection pipe section system. The initial and end positions of the main pipeline system are both slurry pools, and it is a fully enclosed experimental system. The main pipe, which is 150 m in length, has two diameters: 120 mm and 219 mm. The pipe consists of PMMA (polymethylmethacrylate) tubes with a length of 1 m that are used to observe the flow state. Moreover, the main pipe also includes the main slurry pumps, the motors and the control valves, which facilitate transmission. To fully mix the sand and water, a ring cylinder and an agitator pump are arranged in the slurry pool.

The air ejection pipe section system is composed of a jet pump, an air compressor, an air bottle, a nozzle and valves. A branch pipe with a diameter of 90 mm connects to the jet pump and is used to pressurize compressed air. The compressed air is ejected into the main slurry pipe through the filling nozzle.

Fig. 3 displays a comparison between the simulated and experimental pressure gradients for the concentration of 11% in parametric form. As the V_a (gas velocity) changes, the agreement is excellent at different V_s values (slurry velocities). For a slurry velocity of 3.44 m/s, a comparison of the simulated and experimental pressure gradients is shown in Fig. 4. As expected, both the simulated and experimental values monotonically increase with the gas velocity. Although the linearity of the experimental data decreases at high gas velocities, these data display good agreement, with a maximum deviation of 11.25%.

The numerical model can accurately predict the

characteristics of slurry transport with gas injection. Thus, the simulation results at different gas velocities and air ejection angles provide significant reference values.

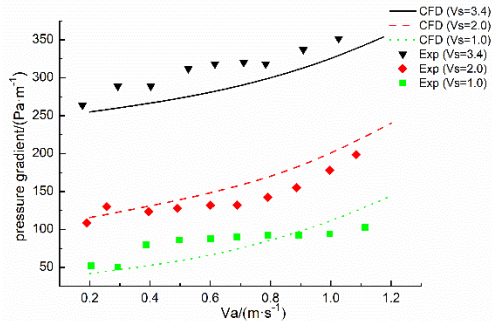


Fig. 3. Comparison of the simulated and experimental data ($C_v=0.11$).

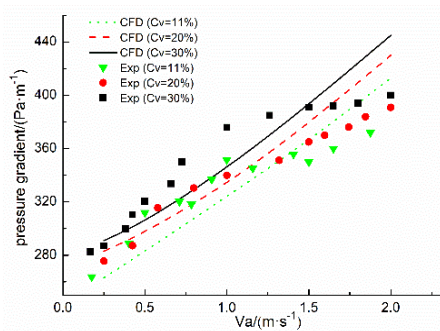


Fig. 4. Comparison of the simulated and experimental data ($V_s=3.44$ m/s).

4.2 Drag Reduction Effect at Different Gas Velocities and Air Ejection Angles

According to the numerical simulation results, at the end of the pipe, a section of 8 meters in length is selected as the focus of the study because the parameters in the preceding flow section are not stable, i.e., full development has not been achieved. In the final step of the transient calculation, the full development stage is reached. Thus, the radial velocity near the central axis approaches zero, and the axial velocity is almost constant.

According to these findings, there is a certain relationship between the wall shear stress and the friction coefficient, and the friction coefficient is an important parameter influenced by the friction resistance. Therefore, the integral mean values of the wall shear stress calculated under different conditions are used to analyze the influence of the gas on the resistance characteristics of the pipeline. As shown in Fig. 5, the broken lines in different plots represent the changes in the wall shear stress at different air ejection angles. The horizontal gray line

represents the transport condition with no gas; therefore, this is the dividing line used to determine whether transport with gas is effective. The points above this gray line indicate that injecting the gas increased resistance, and the points below it indicate a reduction in resistance caused by gas injection.

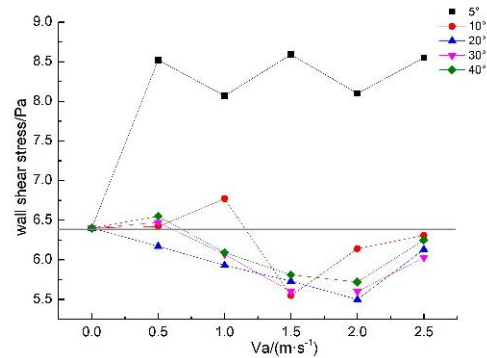


Fig. 5. Wall shear stress under different work conditions.

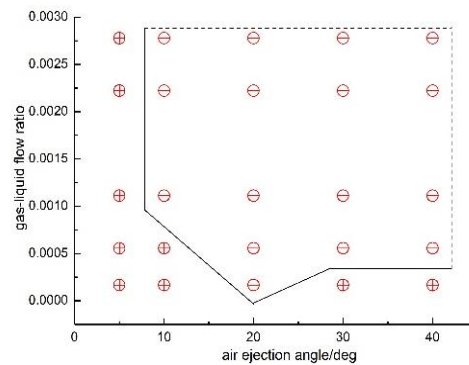


Fig. 6. Parametric diagram of drag reduction.

A reduction in resistance is generated when the air ejection angle is greater than or equal to 10°, and the optimal angle is approximately 20°. The wall shear stress decreases first, then increases with increasing gas velocity and reaches a minimum value between 1.5 m·s⁻¹ and 2.0 m·s⁻¹. The air ejection angle essentially reflects the tendency of gas to rise in the flow. The gas velocity is related to the flow mass and the gas-liquid flow ratio.

A parametric diagram of drag reduction can be constructed according to different working conditions. As shown in Fig. 6, '+' represents a drag increase caused by injecting air, and '-' represents a drag reduction. The solid line is the demarcation between increasing and decreasing drag, and areas outside the dashed line must be verified in subsequent studies. In actual engineering, reducing the drag can be intuitively performed by examining this figure. In addition, 20° is the best choice for the angle of the branch pipe.

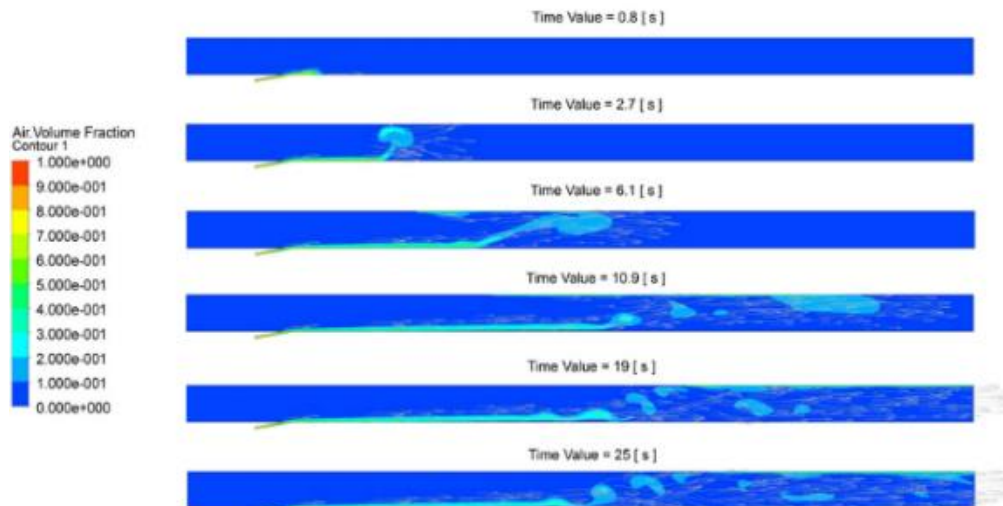


Fig. 7. Evolution of the flow regime ($V_a=2 \text{ m}\cdot\text{s}^{-1}$, $\alpha=20^\circ$).

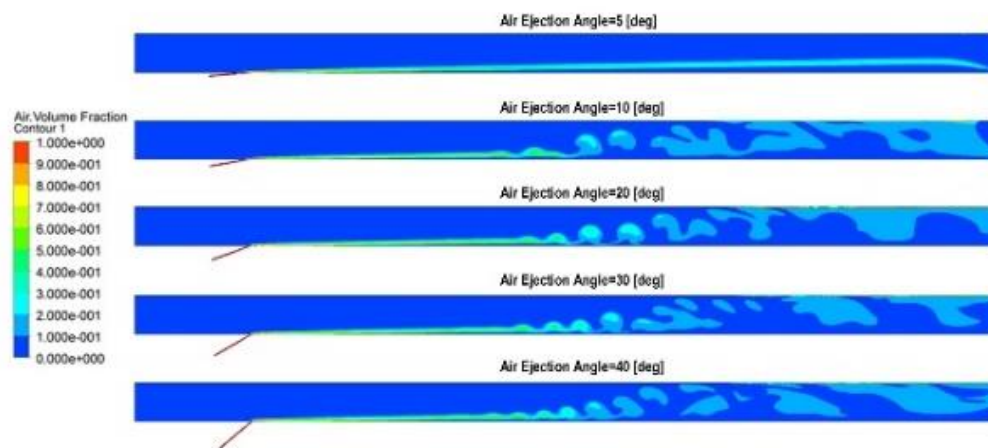


Fig. 8. Flow regime under different air ejection angles ($V_a=2 \text{ m}\cdot\text{s}^{-1}$, time=30 s).

4.3 Analysis of the Flow Regime

The flow regime is analyzed to explore the mechanism of drag reduction associated with injecting air. Fig. 7 illustrates the flow state changes with time. As shown, the bubbles float upward because they are less dense than the slurry. During the floating process, the mixture of bubbles and slurry reduces the wall shear stress. As the mixing time of the slurry and bubbles increases, the gas-covered area of the wall surface of the pipe increases, and more bubbles form, but the distribution of gas within the pipe is inhomogeneous. The gas expands and the bubble bursts in the pipeline at 10.9 s. At 19 s, wavy flow forms at the bottom of the pipe due to the Helmholtz instability between the gas and liquid interfaces (Kim, Padrino, & Joseph, 2011). After 19 s, a stable gas film that reduces the wall roughness

forms below the upper wall of the fully developed section of the pipe.

Fig. 8 indicates the flow regime based on different air ejection angles, and Fig. 9 shows the wall shear stress at the upper and lower wall surfaces. The air flow forms a linear flow field when the air ejection angle is 5° . The bubbles do not disturb the main flow zone, and no gas film forms between the upper wall and slurry. Therefore, as shown in Fig. 9, the wall shear stress at the upper and lower walls is almost the same. In addition, the ejected gas increases the total flow, and the extrusion between the liquid and wall increases, so the wall shear stress increases. This result explains why the resistance increases at an air ejection angle of 5° .

When the air ejection angle changes from 10° to 40° , Fig. 8 clearly shows that a gas film appears at the junction between the slurry and upper wall surface.

In combination with Fig. 9, the wall shear stress between the slurry and upper wall surface obviously decreases, thereby reducing the friction between the wall and the slurry. This result confirms that the formation of the gas film via gas injection is the root cause of drag reduction. In addition, when the air ejection angle is 20°, the wall shear stress sharply decreases and reaches a minimum at 2 m/s.

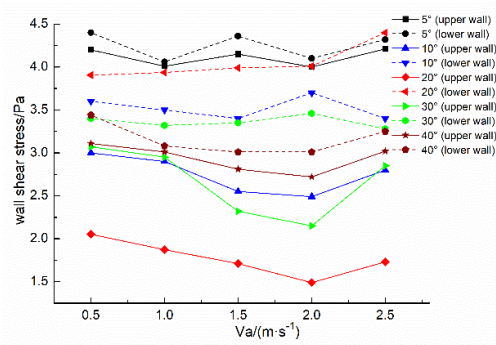


Fig. 9. Wall shear stress under different working conditions.

4.4 Velocity Distribution

($x1-x4$. x coordinate from the gas inlet)

When the flow field in the pipeline reaches a stable regime after bubble injection, the velocity distribution at different distances from the filling port varies. According to the calculation results, the velocity profiles of the slurry -0.65 m, 1.35 m, 12.35 m, and 16.35 m from the gas inlet are plotted, as shown in Fig. 10(a)-(d).

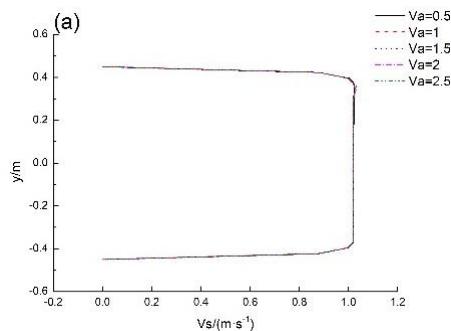


Fig. 10(a). Velocity profile at different locations, $x1=-0.65$.

The position of $x=-0.65$ is the flow field without gas, and it is a critical point. As shown in Fig. 10(a), the velocity distribution is stable and has obvious boundary layer regions and clear mainstream regions. Thus, the interaction between the bubbles and slurry does not affect this flow field. As shown

in Fig. 10(b), $x=1.35$ is the position at which the gas just passes into the pipe, and the effect of bubble injection on the slurry velocity distribution is limited to the bottom of the pipe. The effect strengthens with increasing gas velocity, but there is almost no influence on the velocity distribution in the upper part of the pipe. The sudden change in velocity is mainly caused by the momentum exchange between the gas and slurry flowing at the bottom of the pipe.

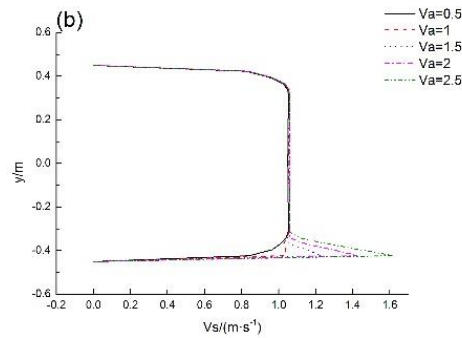


Fig. 10(b). Velocity profile at different locations, $x2=1.35$.

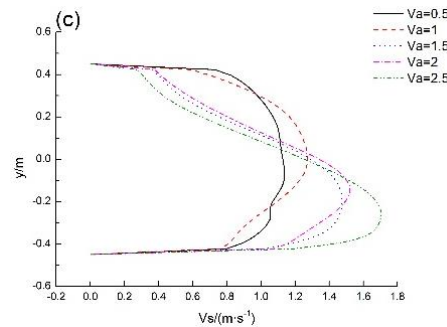


Fig. 10(c). Velocity profile at different locations, $x3=12.35$.

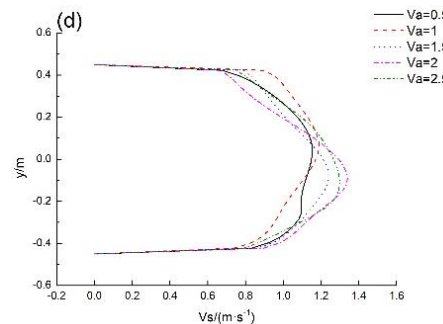


Fig. 10(d). Velocity profile at different locations, $x4=16.35$.

As illustrated in Fig. 10(c), the velocity distribution at $x=12.35$ is notably affected by the gas. The gas position fluctuates, and some gas floats at this position, causing the original flow pattern to change. Therefore, the velocity curve is distorted. As shown

in Fig. 10(d), the velocity vector at $x = 16.35$ is almost axial, and the effect of the gas on transverse movement is limited. The developed flow has formed, and the bubbles only have a beneficial effect on the flow. In addition, the distortion of the velocity curve in the mainstream area disappears, and the velocity curve is relatively symmetric. After a certain period, the gas that produces an unstable turbulence effect does not continuously interact with the slurry, and the flow restabilizes.

4.5 Pressure Distribution

At a distance of 9.35 m from the gas inlet, the pressure inside the pipe changes with time. The pressure fluctuations are initially obvious, and at the start of the injection, the gas movement is irregular and unstable. When the gas is ejected for a period of time, the pressure fluctuation range is maintained at a stable level. Therefore, the ejected gas does not affect the transport stability when the flow is stable. Moreover, no extra energy is produced, and the flow is not hindered.

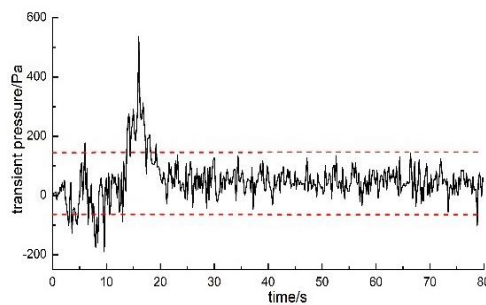


Fig. 11. Pressure fluctuations in the pipeline.

5. CONCLUSIONS

A numerical simulation of the parameters involved in the pneumatic regulation of slurry in horizontal pipeline transport is conducted in this study, and the experiment is verified by an aerated transport test. The simulated results are in good agreement with the experimental results. The experiment is performed using a gas-ejected pipeline apparatus. Taking various sensitive factors (air ejection angle and gas velocity) as variables, the resistance characteristics, flow state and transport stability are simulated and analyzed. The conclusions are as follows.

Injected gas has a drag reduction effect on the slurry transport under certain working conditions. The resistance characteristic line is a concave curve with an optimum drag reduction rate point at which the air ejection angle is approximately 20° and the gas velocity ranges between $1.5 \text{ m}\cdot\text{s}^{-1}$ and $2.0 \text{ m}\cdot\text{s}^{-1}$.

The gas film that forms at the pipe wall is the root cause of the drag reduction. After injecting gas into

the pipe, the distortion of the velocity curve reflects the drag reduction in the fully developed flow section. The bubbles expand when the gas is ejected into the pipe. When the flow reaches a fully developed state, the bubbles float below the upper pipe wall and form a gas film between the upper wall and the slurry. The gas film reduces the friction between the slurry and the wall surface, which causes the wall shear stress to decrease, resulting in a drag reduction.

The gas entering the pipeline disturbs the stability of the flow in a short time, but the velocity field and the pressure field tend to be stable after the flow becomes fully developed. According to the analyses of the velocity and pressure in the flow field under different working conditions, the flow with gas is stable in the pipeline, and a drag reduction is achieved without damaging the transport equipment. Therefore, the results in this paper can be applied in real-world cases.

ACKNOWLEDGMENTS

This research work is supported by the National Natural Science Foundation of China (Grant No. 51709210) and the Excellent Dissertation Cultivation Funds of Wuhan University of Technology (Grant No. 2017-YS-038)

REFERENCES

- Ali, B. A. and S. Pushpavanam (2011). Analysis of unsteady gas-liquid flows in a rectangular tank: Comparison of Euler-Eulerian and Euler-Lagrangian simulations. *International Journal of Multiphase Flow* 37(3),268-277.
- Aliseda, A. and J. C. Lasheras (2006). Effect of buoyancy on the dynamics of a turbulent boundary layer laden with microbubbles. *Journal of Fluid Mechanics* 559, 307.
- Bjerkholt, J. T., T. R. Cumby and I. M. Scotford (2005). The Effects of Air Injection on the Pipeline Transport of Cattle and Pig Slurries. *Biosystems Engineering* 91(3), 361-368.
- Casas, E. and L. A. Fernández (1989). A Green's formula for quasilinear elliptic operators. *Journal of Mathematical Analysis & Applications* 142(1), 62-73.
- Gidaspow, D., R. Bezburuah and J. Ding (1991). Hydrodynamics of circulating fluidized beds: Kinetic theory approach. Paper presented at the 7th international conference on fluidization, Gold Coast (Australia), 3-8 May 1992.
- Gillies, R. G., M. J. Mckibben and C. A. Shook (1996). Pipeline flow of gas liquid and sand

- mixtures at low velocities. *Particulate Science & Technology* 14(4), 293-314.
- Gopaliya, M. K. and D. R. Kaushal (2015). Analysis of Effect of Grain Size on Various Parameters of Slurry Flow through Pipeline Using CFD. *Particulate Science & Technology* 33(4), 369-384.
- Heywood, N. I. and M. E. Charles (1979). The stratified flow of gas and non-newtonian liquid in horizontal pipes. *International Journal of Multiphase Flow* 5(5), 341-352.
- Hoogendoorn, C. J. (1959). Gas-liquid flow in horizontal pipes. *Chemical Engineering Science* 9(4), 205-217.
- Jameson, A. and D. Mavriplis (1985). Finite volume solution of the two-dimensional Euler equations on a regular triangular mesh. *Aiaa Journal* 24(4), 611-618.
- Kaushal, D. R., T. Thinglas, Y. Tomita, S. Kuchii and H. Tsukamoto (2012). CFD modeling for pipeline flow of fine particles at high concentration. *International Journal of Multiphase Flow* 43, 85-100.
- Kim, H., J. C. Padrino and D. D. Joseph (2011). Viscous effects on Kelvin–Helmholtz instability in a channel. *Journal of Fluid Mechanics* 680(680), 398-416.
- Lockhart, R. W. and R. C. Martinelli (1949). Proposed Correlation of Data for Isothermal Two-Phase , Two-Component Flow in Pipelines. *CHEmical Engineering Progress* 45, 39-48.
- Lun, C. K. K., S. B. Savage, D. J. Jeffrey and N. Chepuruiy (2006). Kinetic theories for granular flow: inelastic particles in Couette flow and slightly inelastic particles in a general flow field. *Journal of Fluid Mechanics* 140(140), 223-256.
- Marié, J.-L. (1987). A simple analytical formulation for microbubble drag reduction. *Physico Chemical Hydrodynamics* 8(2), 213-220.
- Messa, G. V. and S. Malavasi (2015). Improvements in the numerical prediction of fully-suspended slurry flow in horizontal pipes. *Powder Technology* 270, 358-367.
- Messa, G. V., M. Malin and S. Malavasi (2014). Numerical prediction of fully-suspended slurry flow in horizontal pipes. *Powder Technology* 256(256), 61-70.
- Miedema, S. A. (2016). The heterogeneous to homogeneous transition for slurry flow in pipes. *Ocean Engineering* 123, 422-431.
- Orell, A. (2005). Experimental validation of a simple model for gas–liquid slug flow in horizontal pipes. *Chemical Engineering Science* 60(5), 1371-1381.
- Orell, A. (2007). The effect of gas injection on the hydraulic transport of slurries in horizontal pipes. *Chemical Engineering Science* 62(23).
- Sanders, W. C., E. S. Winkel and D. R. Dowling, M. Perlin and S. L. Ceccio (2006). Bubble friction drag reduction in a high-Reynolds-number flat-plate turbulent boundary layer. *Journal of Fluid Mechanics* 552(-1), 353.
- Srivastava, R. P. S. and G. S. R. Narasimhamurty (1973). Hydrodynamics of non-Newtonian two-phase flow in pipes. *Chemical Engineering Science* 28(2), 553-558.